

Nucleon spin structure

Wei Zhu and Jianhong Ruan

Department of Physics, East China Normal University, Shanghai 200062, P.R. China

Abstract

This paper contains three parts relating to the nucleon spin structure in a simple picture of the nucleon: (i) The polarized gluon distribution in the proton is dynamically predicted starting from a low scale by using a nonlinear QCD evolution equation-the DGLAP equation with the parton recombination corrections, where the nucleon is almost only consisted of valence quarks. We find that the contribution of the gluon polarization to the nucleon spin structure is much larger than the predictions of most other theories. This result suggests a significant orbital angular momentum of the gluons is required to balance the gluon spin momentum; (ii) The spin structure function g_1^p of the proton is studied, where the perturbative evolution of parton distributions and nonperturbative Vector Meson Dominance (VMD) model are used. We predict g_1^p asymptotic behavior at small x from lower Q^2 to higher Q^2 . The results are compatible with the data including the HERA early estimations and COMPASS new results; (iii) The generalized Gerasimov-Drell-Hearn (GDH) sum rule is understood based on the polarized parton distributions of the proton with the higher twist contributions. A simple parameterized formula is proposed to clearly present the contributions of different components in the proton to $\Gamma_1^p(Q^2)$. The results suggest a possible extended objects with size $0.2 - 0.3 fm$ inside the proton.

PACS number(s): 12.38.Cy, 12.38.Qk, 12.38.Lg, 12.40.Vv

keywords: Nucleon spin structure

1 Introduction

A precise determination of the polarized gluon distribution $\delta g(x, Q^2)$ is important in order to understand the spin structure of the nucleon. However, the direct measurement of the polarized gluon distribution in the nucleon is difficult. In the global analysis of the polarized lepton-nucleon deep inelastic scattering (DIS), the distribution $\delta g(x, Q^2)$ is extracted from the spin structure function $g_1(x, Q^2)$ through scaling violation as a higher-order effect of quantum chromodynamics (QCD). Unfortunately, such indirect determination of $\delta g(x, Q^2)$ is affected by large uncertainties because of the limited range in momentum transfer at fixed Bjorken- x and almost entirely arbitrary input gluon distribution. In fact, the data suggest that such global fit with either positive or negative input gluon distributions provides equally good agreement. Recently, a high-precision measurement of the mid-rapidity polarized proton-proton (p-p) collisions stringently constraint the polarized parton distribution functions mentioned above. The analysis of NNPDF collaboration [1] found an evidence for possible larger gluon spin distribution, which is against the common belief that it is rather small.

In Sec. 2 of this work we use a QCD dynamic model of the parton distributions to predict the polarized gluon distribution in the proton without unknown input gluon distribution. Our model imagines that all gluons in the nucleon are radiated from the intrinsic quarks beginning at a low resolution scale. Thus, we can predict the radiative (unpolarized and polarized) gluon distributions provided the initial quark distributions are fixed. Such quark model was early proposed by [2,3,4] in 1977, it was improved in our previous work [5,6], where the Dokshitzer-Gribov-Lipatov-Altarelli-Parisi (DGLAP) equation [7,8,9] with the parton recombination corrections is used to reproduce the unpolarized parton distributions of the nucleon at $Q^2 > 1\text{GeV}^2$ [10,11,12]. Since the similar corrections of the parton recombination to the polarized DGLAP equation have been proposed in work [13], we can use these two modified evolution equations to predict the polarized gluon distribution in the proton dynamically.

Comparing with the global analysis via scaling violation, the polarized gluon distribution in this work is determined directly by the observed spin structure function $g_1(x, Q^2)$. We find that the contribution of the gluon polarization to the nucleon spin structure is surprisingly large, which is in excess of the previous estimations in theory. The reasons are as following: (i) The shadowing effect of the gluon recombination in the evolution of the polarized parton distributions is weaker than that in the unpolarized case since $g\delta g \ll g^2$ at small x . Therefore, much more strong polarized gluons are emitted by quarks inside the polarized proton through a long evolution length from μ^2 to $Q^2 > 1\text{GeV}^2$; (ii) The positive contribution of the polarized gluon recombination, which is opposite to that of the unpolarized gluon recombination enhance the accumulation of the gluon helicity. The QCD evolution of the parton distributions begins from a low bound state scale μ^2 not

only dynamically determine the polarized gluon distribution, but also exposes a novel spin-orbital structure of the nucleon in the light-cone frame, where the nucleon spin crisis has a possible explanation.

Concerning the spin structure function, recently COMPASS experiment at CERN collected a large number of events of polarized inelastic scattering off the protons with very small x [14]. The preliminary analysis of these data combining with the previous experiments [15,16,17,18], showed non zero and positive asymptotic structure function g_1^p . In these fixed target experiments the low values of x are almost reached by lowering the values of Q^2 . The knowledge of the nucleon spin structure function $g_1(x, Q^2)$ at low Q^2 and small x is particularly interesting, since it is not only an important information to resolve the "proton spin crisis", but also provides us with a good place to study the transition from the perturbative research to the nonperturbative description of the proton structure.

In Sec. 3 we try to study the behavior of g_1^p at small x but in the full Q^2 range. As we know that the structure functions of the nucleon are mainly constructed of the parton distributions at $Q^2 > 1\text{GeV}^2$, while the nonperturbative contributions to the structure functions become un-negligible at $Q^2 \ll 1\text{GeV}^2$. A key question is what components construct the spin structure functions of the proton at such low Q^2 ? Particularly, do the parton distributions and their pQCD evolution still play a role or not? To answer these questions, we discuss the application of the DGLAP equation with the parton recombination corrections at low Q^2 in detail. We point out that the isolation of the contributions of the vector meson is necessary for keeping the factorization schema of the polarized parton distributions at low Q^2 . We find two different asymptotic behaviors of g_1^p at $x < 10^{-3}$: nonperturbative behavior $\sim x^{-1}$ at $Q^2 < 1\text{GeV}^2$ and perturbative drop at $Q^2 > 3\text{GeV}^2$. We predict the translation of g_1^p at small x from lower Q^2 to higher Q^2 . The results are compatible with the data including the early HERA estimations and COMPASS new results. We point out that the measurements at different x with different values of Q^2 in the fixed target experiments mix the complicated asymptotic behavior of g_1^p . The predicted strong Q^2 - and x -dependence of g_1^p at $0.01 < Q^2 < 3\text{GeV}^2$ and $x < 0.1$ due to the mixture of nonperturbative vector meson interactions and the QCD evolution of the parton distributions can be checked on the next Electron-Ion Collider (EIC).

There is particular interest in the first moment $\Gamma_1(Q^2) = \int_0^1 dx g_1(x, Q^2)$ of the spin structure functions $g_1(x, Q^2)$, which has been measured from high Q^2 down to $\sim 0\text{GeV}^2$. The goal to obtain universal expressions describing $\Gamma_1(Q^2)$ at any Q^2 is an attractive task for both theoretical and phenomenological point of view. In theory, $\Gamma_1(0)$ is constrained by the Gerasimov-Drell-Hearn (GDH) sum rule [19,20]. In Sec. 4 we try to expose the partonic structure in the GDH sum rule. Since we have known the contributions of $g_1^{DGLAP+ZRS}$ and g_1^{VMD} , one can expose the properties of $\Gamma_1^{HT}(Q^2)$ after subtracting

these two contributions from the experimental data about $\Gamma_1^p(Q^2)$. This opens a window to visit higher twist effects at low Q^2 in the nucleon structure. We proposed a simple parameterized form of $\Gamma_1^p(Q^2)$. We find that the negative twist-4 effect dominates the suppression of $\Gamma_1^p(Q^2)$ at $Q^2 < 1\text{GeV}^2$, while both the twist-4 and twist-6 effects have a dramatic change of $\Gamma_1^p(Q^2)$ at $Q^2 \sim 1\text{GeV}^2$, which suggest a possible extended objects with size $0.2 - 0.3\text{ fm}$ inside the proton.

Finally, following the above mentioned discussions, we will give a summary in Sec.5.

2 Dynamical determination of gluon helicity distribution in the nucleon

2.1 Nonlinear polarized QCD evolution equation

We use $f_+(x, Q^2)$ and $f_-(x, Q^2)$ to refer to parton ($f = q, \bar{q}, g$) densities with positive and negative helicity which carry a fraction x of the nucleon momentum. The difference $\delta f(x, Q^2) = f_+(x, Q^2) - f_-(x, Q^2)$ measures how much the parton of flavor f remembers its parent's nucleon polarization. The spin averaged parton densities are given by $f(x, Q^2) = f_+(x, Q^2) + f_-(x, Q^2)$.

The spin-dependent QCD evolution equation of parton distributions with parton recombination corrections was first derived by Zhu, Shen and Ruan (ZRS) in [13], it reads

$$\begin{aligned} & Q^2 \frac{dx \delta q_v(x, Q^2)}{dQ^2} \\ &= \frac{\alpha_s(Q^2)}{2\pi} \int_x^1 \frac{dy}{y} \frac{x}{y} y \delta q_v(y, Q^2) \Delta P_{qq}\left(\frac{x}{y}\right), \end{aligned} \quad (2.1.1)$$

for flavor non-singlet quarks;

$$\begin{aligned} & Q^2 \frac{dx \delta q_i(x, Q^2)}{dQ^2} \\ &= \frac{\alpha_s(Q^2)}{2\pi} \int_x^1 \frac{dy}{y} \frac{x}{y} [y \delta q_i(y, Q^2) \Delta P_{qq}\left(\frac{x}{y}\right) + y \delta g(y, Q^2) \Delta P_{qg}\left(\frac{x}{y}\right)] \\ &\quad - \frac{\alpha_s^2(Q^2)}{4\pi R^2 Q^2} \int_x^{1/2} \frac{dy}{y} x \Delta P_{gg \rightarrow q}(x, y) [y g(y, Q^2) y \delta g(y, Q^2)] \\ &\quad + \frac{\alpha_s^2(Q^2)}{4\pi R^2 Q^2} \int_{x/2}^x \frac{dy}{y} x \Delta P_{gg \rightarrow q}(x, y) [y g(y, Q^2) y \delta g(y, Q^2)], \quad (if \ x \leq 1/2), \\ & Q^2 \frac{dx \delta q_i(x, Q^2)}{dQ^2} \\ &= \frac{\alpha_s(Q^2)}{2\pi} \int_x^1 \frac{dy}{y} \frac{x}{y} [y \delta q_i(y, Q^2) \Delta P_{qq}\left(\frac{x}{y}\right) + y \delta g(y, Q^2) \Delta P_{qg}\left(\frac{x}{y}\right)] \\ &\quad + \frac{\alpha_s^2(Q^2)}{4\pi R^2 Q^2} \int_{x/2}^{1/2} \frac{dy}{y} x \Delta P_{gg \rightarrow q}(x, y) [y g(y, Q^2) y \delta g(y, Q^2)], \quad (if \ 1/2 \leq x \leq 1), \end{aligned} \quad (2.1.2)$$

for sea quarks;

$$\begin{aligned} & Q^2 \frac{dx \delta g(x, Q^2)}{dQ^2} \\ &= \frac{\alpha_s(Q^2)}{2\pi} \int_x^1 \frac{dy}{y} \frac{x}{y} [y \sum_{i=1}^{2f} \delta q_i(y, Q^2) \Delta P_{qg}\left(\frac{x}{y}\right) + y \delta g(y, Q^2) \Delta P_{gg}\left(\frac{x}{y}\right)] \end{aligned}$$

$$\begin{aligned}
& -\frac{\alpha_s^2(Q^2)}{4\pi R^2 Q^2} \int_x^{1/2} \frac{dy}{y} x \Delta P_{gg \rightarrow g}(x, y) [yg(y, Q^2) y \delta g(y, Q^2)] \\
& + \frac{\alpha_s^2(Q^2)}{4\pi R^2 Q^2} \int_{x/2}^x \frac{dy}{y} x \Delta P_{gg \rightarrow g}(x, y) [yg(y, Q^2) y \delta g(y, Q^2)], (if \ x \leq 1/2), \\
& Q^2 \frac{dx \delta g(x, Q^2)}{dQ^2} \\
& = \frac{\alpha_s(Q^2)}{2\pi} \int_x^1 \frac{dy}{y} \frac{x}{y} [y \sum_{i=1}^{2f} \delta q_i(y, Q^2) \Delta P_{qq}(\frac{x}{y}) + y \delta g(y, Q^2) \Delta P_{gg}(\frac{x}{y})] \\
& + \frac{\alpha_s^2(Q^2)}{4\pi R^2 Q^2} \int_{x/2}^{1/2} \frac{dy}{y} x \Delta P_{gg \rightarrow g}(x, y) [yg(y, Q^2) y \delta g(y, Q^2)], (if \ 1/2 \leq x \leq 1) \quad (2.1.3)
\end{aligned}$$

for gluon, where the factor $1/(4\pi R^2)$ is from the normalization of two-parton distribution, R is the correlation length of two initial partons, the linear terms are the standard spin-dependent DGLAP evolution and the recombination functions in the nonlinear terms are (see appendix A)

$$\Delta P_{gg \rightarrow g}(x, y) = \frac{27}{64} \frac{(2y - x)(-20y^3 + 12y^2x - x^3)}{y^5}, \quad (2.1.4)$$

$$\Delta P_{gg \rightarrow q}(x, y) = \frac{1}{48} \frac{(2y - x)^2(-y + x)}{y^4}. \quad (2.1.5)$$

The spin structure function g_1 at leading order (LO) and $Q^2 > 1 \text{ GeV}^2$ is written as

$$g_1(x, Q^2) = \frac{1}{2} \sum_i e_i^2 [\delta q_i(x, Q^2) + \delta \bar{q}_i(x, Q^2)], \quad (2.1.6)$$

where e_i is the electric charge of the (light) quark of flavor i , $i = u, d, s$.

The solutions of Eqs (2.1.1-2.1.3) are coupled with the spin-averaged evolution equations, which are

$$\begin{aligned}
& Q^2 \frac{dx q_v(x, Q^2)}{dQ^2} \\
& = \frac{\alpha_s(Q^2)}{2\pi} \int_x^1 \frac{dy}{y} \frac{x}{y} y q_v(y, Q^2) P_{qq}(\frac{x}{y}), \quad (2.1.7)
\end{aligned}$$

for valence quarks;

$$\begin{aligned}
& Q^2 \frac{dx q_i(x, Q^2)}{dQ^2} \\
& = \frac{\alpha_s(Q^2)}{2\pi} \int_x^1 \frac{dy}{y} \frac{x}{y} [y q_i(y, Q^2) P_{qq}(\frac{x}{y}) + y g(y, Q^2) P_{qg}(\frac{x}{y})] \\
& \quad - \frac{\alpha_s^2(Q^2)}{4\pi R^2 Q^2} \int_x^{1/2} \frac{dy}{y} x P_{gg \rightarrow q}(x, y) [yg(y, Q^2)]^2
\end{aligned}$$

$$\begin{aligned}
& + \frac{\alpha_s^2(Q^2)}{4\pi R^2 Q^2} \int_{x/2}^x \frac{dy}{y} x P_{gg \rightarrow q}(x, y) [yg(y, Q^2)]^2, (if \ x \leq 1/2), \\
& Q^2 \frac{dx q_i(x, Q^2)}{dQ^2} \\
& = \frac{\alpha_s(Q^2)}{2\pi} \int_x^1 \frac{dy}{y} \frac{x}{y} [y q_i(y, Q^2) P_{qq}(\frac{x}{y}) + yg(y, Q^2) P_{qg}(\frac{x}{y})] \\
& + \frac{\alpha_s^2(Q^2)}{4\pi R^2 Q^2} \int_{x/2}^{1/2} \frac{dy}{y} x P_{gg \rightarrow q}(x, y) [yg(y, Q^2)]^2, (if \ 1/2 \leq x \leq 1), \tag{2.1.8}
\end{aligned}$$

for sea quarks;

$$\begin{aligned}
& Q^2 \frac{dx g(x, Q^2)}{dQ^2} \\
& = \frac{\alpha_s(Q^2)}{2\pi} \int_x^1 \frac{dy}{y} \frac{x}{y} [y \sum_{i=1}^{2f} q_i(y, Q^2) P_{qq}(\frac{x}{y}) + yg(y, Q^2) P_{gg}(\frac{x}{y})] \\
& \quad - \frac{\alpha_s^2(Q^2)}{4\pi R^2 Q^2} \int_x^{1/2} \frac{dy}{y} x P_{gg \rightarrow g}(x, y) [yg(y, Q^2)]^2 \\
& \quad + \frac{\alpha_s^2(Q^2)}{4\pi R^2 Q^2} \int_{x/2}^x \frac{dy}{y} x P_{gg \rightarrow g}(x, y) [yg(y, Q^2)]^2, (if \ x \leq 1/2), \\
& Q^2 \frac{dx g(x, Q^2)}{dQ^2} \\
& = \frac{\alpha_s(Q^2)}{2\pi} \int_x^1 \frac{dy}{y} \frac{x}{y} [y \sum_{i=1}^{2f} q_i(y, Q^2) P_{qq}(\frac{x}{y}) + yg(y, Q^2) P_{gg}(\frac{x}{y})] \\
& \quad + \frac{\alpha_s^2(Q^2)}{4\pi R^2 Q^2} \int_{x/2}^{1/2} \frac{dy}{y} x P_{gg \rightarrow g}(x, y) [yg(y, Q^2)]^2, (if \ 1/2 \leq x \leq 1) \tag{2.1.9}
\end{aligned}$$

for gluon, where the linear terms are the standard DGLAP evolution [7,8,9] and the recombination functions in the nonlinear terms are [10,11,12]

$$P_{gg \rightarrow g}(x, y) = \frac{9}{64} \frac{(2y - x)(72y^4 - 48xy^3 + 140x^2y^2 - 116x^3y + 29x^4)}{xy^5}, \tag{2.1.10}$$

$$P_{gg \rightarrow q}(x, y) = P_{gg \rightarrow \bar{q}}(x, y) = \frac{1}{96} \frac{(2y - x)^2(18y^2 - 21xy + 14x^2)}{y^5}. \tag{2.1.11}$$

2.2 Dynamically radiative polarized gluon distribution

We focus on the gluon distribution, its evolution is dominated by the valence quark distributions. Therefore, the corrections of the asymmetry sea distributions in the nucleon are neglected in this work.

As we know, there are many effective QCD theories which describe the nucleon as a bound state of three quarks in its rest frame. The distributions of these quarks in the light-cone configuration have a similar character as the valence quark distributions observed at high Q^2 in DIS. Besides, the QCD evolution equation shows that either the second moment (i.e., the average momentum fraction) of the unpolarized gluon distribution or the first moment (i.e., the total helicity) of the polarized gluon distribution increase as Q^2 increasing. A natural suggestion is that all partons (valence quarks, sea quarks and gluons) at high Q^2 scale are evolved from three initial valence quarks via QCD dynamics. Such idea was first proposed in 1977 for unpolarized parton distributions by [2,3,4]. They assumed that the nucleon consists of valence quarks at a low starting point $\mu^2 \sim 0.064 GeV^2$ (but is still in the perturbative region $\alpha_s(\mu^2)/2\pi < 1$ and $\mu > \Lambda_{QCD}$), and the gluons and sea quarks are produced at $Q^2 > \mu^2$ using the DGLAP equation. However, such natural input is failed due to the too steep behavior of the predicted parton distributions at small x since a long evolution distance from μ^2 to $Q^2 > 1 GeV^2$. Recently the above naive idea was realized in the unpolarized DGLAP equation with the parton recombination corrections at LO approximation in [5,6], where the input distributions at $\mu^2 = 0.064 GeV^2$ were extracted through fitting $F_2^{p,n}(x, Q^2)$ and they have been fixed as

$$xu_v(x, \mu^2) = 24.3x^{1.98}(1-x)^{2.06}, \quad (2.2.1)$$

$$xd_v(x, \mu^2) = 9.10x^{1.31}(1-x)^{3.8}, \quad (2.2.2)$$

while

$$g(x, \mu^2) = 0, \quad q_i(x, \mu^2) = \bar{q}_i(x, \mu^2) = 0, \quad (2.2.3)$$

and the parameters in Eqs. (2.1.8) and (2.1.9) are $\Lambda_{QCD} = 0.204 GeV$ and $R = 4.24 GeV^{-1}$. We plot these input distributions in Fig.1.

Similarly, using the polarized DGLAP equation with the parton recombination corrections Eqs. (2.1.1)-(2.1.3) and combining Eqs. (2.1.7)-(2.1.9), we fit $g_1^{p,n}(x, Q^2)$ with the data [21] in Fig.2, and extract the input polarized valence quark distributions in the proton as

$$\delta u_v(x, \mu^2) = 40.3x^{2.85}(1-x)^{2.15}, \quad (2.2.4)$$

$$\delta d_v(x, \mu^2) = -18.22x^{1.41}(1-x)^{4.0}, \quad (2.2.5)$$

and

$$\delta g(x, \mu^2) = 0, \quad \delta q_i(x, \mu^2) = \delta \bar{q}_i(x, \mu^2) = 0, \quad (2.2.6)$$

they are plotted in Fig.1.

We predict the polarized gluon distribution at different Q^2 in Fig. 3. The results clearly show the accumulation of polarized gluons at small x .

There are several databases of the polarized parton distributions, which are extracted by the global fitting DIS data. For example, we compare our results with the GRV distribution [22] in Fig. 4. The difference is obvious. It is not surprise that the polarized gluon distribution has large uncertainty, since the shape of the input gluon distribution is not constrained well enough by the DIS data alone.

In order to understand the contribution of large gluon polarization, we draw the evolution kernels $P_{qg}(z)$, $P_{gg}(z)$, $\Delta P_{qg}(z)$, $\Delta P_{gg}(z)$ and $yP_{gg \rightarrow g}(z)$, $yP_{gg \rightarrow q}(z)$, $y\Delta P_{gg \rightarrow g}(z)$, $y\Delta P_{gg \rightarrow q}(z)$ in Figs. 5 and 6. One can find that

- (i) $P_{gg}(z) > 0$ and $\Delta P_{gg}(z) > 0$ imply that $\delta g(x, Q^2)$ is positive in our dynamic model;
- (ii) Since $\Delta P_{qg}(z) < 0$ at small z , we have $dg_1(x, Q^2)/d \ln Q^2 \sim -\delta g(x, Q^2)$ at small x , i.e., a large positive δg at small x is expected to drive g_1 towards large negative values;
- (iii) $\Delta P_{gg \rightarrow g} < 0$ and $\Delta P_{gg \rightarrow q} < 0$ lead the net positive corrections of the gluon fusion to the polarized parton distributions since a negative sign in the shadowing terms of Eq. (2.1.3). To illustrate this effect, in Fig.7 we present $x\delta g(x, Q^2)$ with and without the corrections of gluon recombination corrections at $Q^2 = 1$ and $5GeV^2$. One can find that the effects of the gluon recombination in the polarized gluon distribution is positive.

As we know that some approaches are planned to measure the gluon distributions. For example, the semi-inclusive deep inelastic scattering processes measure the $\delta g/g$ from helicity asymmetry in photon-gluon fusion. The COMPASS collaboration [23] have used this method and found a rather small value for $\delta g/g = 0.024 \pm 0.080 \pm 0.057$ at $x = 0.09$ and $Q^2 = 3GeV^2$. However we think that although the value of $\delta g/g$ is small, the polarized gluon contribution to the spin of the nucleon may be sizable since g itself is large at small x . In order to compare with the data, one needs to assume a suitable form for the unpolarized gluon distribution $g(x, Q^2)$. Fortunately, both $\delta g(x, Q^2)$ and $g(x, Q^2)$ are calculated within a same dynamics in this work and we avoid a larger uncertainty in the determination of $g(x, Q^2)$. We compare our predicted $\delta g/g$ with the COMPASS data in Fig. 8.

The other direct probing of δg is offered by jet and π production in polarized proton-proton collisions available at BNL Relativistic Heavy Ion Collider (RHIC). A recent DSSV analysis [24] of high-statistics 2009 STAR [25] and PHENIX [26] data showed an evidence

of non-zero gluon helicity in the proton. They found that the polarized gluon distribution in the proton is positive and away from zero in $0.05 < x < 0.2$, although the presented data has very large uncertainty at small x region. Figure 9 presents the comparisons of our predicted $g_1^p(x, Q^2)$ at $Q^2 = 10\text{GeV}^2$ with the DSSV bounds. Our results are beyond a up bound of the DSSV results, however, a sizable gluon polarization is still possible if taking the 90% confidence level (C.L.) interval.

The NNPDF group has developed a new methodology [1] to extract polarized gluon distribution function. They used all essential available data and got an evidence of positive gluon polarization in the medium and small x region. This discovery is compatible with our results. Figure 10 shows the comparison of our predicted polarized gluon distribution with the NNPDF bounds. This example shows that a positive initial distribution of the polarized gluon at μ^2 in the nucleon is impossible since it will obviously go beyond the up bound of the NNPDF analysis at $Q^2 \sim 10\text{GeV}^2$.

2.3 Discussions

The total helicity of partons in a polarized proton are calculated by the first moments

$$\Delta f(Q^2) = \int_0^1 dx \delta f(x, Q^2), \quad (2.3.1)$$

Note that our predicted $\Delta q_s(Q^2)$ for the sea quarks is positive since the negative contributions from the asymmetric strange quarks are neglected in this work.

The contribution of quark polarization to the proton spin $\Delta\Sigma(Q^2 = 5\text{GeV}^2) \simeq 0.30$ in our estimation. It is interesting that this value is compatible with the world average values $\Delta\Sigma(Q^2 = 10\text{GeV}^2) = 0.31 \pm 0.07$ [27], and $\Delta\Sigma(Q^2 = 5\text{GeV}^2) = 0.333 \pm 0.011 \pm 0.025 \pm 0.028$ [28].

In Fig. 11 we plot the evolutions of $\Delta\Sigma(Q^2)$ and $\Delta g(Q^2)$ with increasing Q^2 . We find that $\Delta q_v(Q^2) = 0.296$, but $\Delta q_s(Q^2)$ is slowly increasing from 0 at μ^2 to 0.016 at $Q^2 = 1000\text{GeV}^2$ due to the parton recombination corrections. On the other hand, the gluon helicity $\Delta g(Q^2)$ increases with $\ln Q^2$ beginning from zero at μ^2 , and becomes large when $Q^2 > 0.3\text{GeV}^2$.

The above mentioned $\Delta\Sigma$ and Δg should be balanced by the orbital angular momenta of partons. For this sake, we write the nucleon helicity sum rule

$$\frac{1}{2} = \frac{1}{2}\Delta\Sigma(Q^2) + \Delta g(Q^2) + \sum_q L_q^z(Q^2) + L_g^z(Q^2), \quad (2.3.2)$$

where $L_{q,g}^z$ denote the contributions of orbital angular momenta of quarks and gluons. In our model the sum rule at $Q^2 = \mu^2$ is

$$\frac{1}{2} = \frac{1}{2}\Delta\Sigma(\mu^2) + \sum_q L_q^z(\mu^2), \quad (2.3.3)$$

where

$$\Delta\Sigma(\mu^2) = \Delta u_v(\mu^2) + \Delta d_v(\mu^2), \quad (2.3.4)$$

$$\sum_q L_q^z(\mu^2) = L_u^z(\mu^2) + L_d^z(\mu^2). \quad (2.3.5)$$

On the other hand, the helicity sum rule of the polarized proton in its rest frame according to the constituent quark model is

$$\frac{1}{2} = \frac{1}{2} \sum_q \Delta q^c, \quad (2.3.6)$$

where Δq^c denotes the quark polarization in the quark model.

Comparing Eq. (2.3.6) with Eq. (2.3.3), we assume

$$\frac{1}{2}\Delta u^c = \frac{1}{2}\Delta u_v(\mu^2) + L_{u_v}^z(\mu^2),$$

and

$$\frac{1}{2}\Delta d^c = \frac{1}{2}\Delta d_v(\mu^2) + L_{d_v}^z(\mu^2), \quad (2.3.7)$$

where the motions of partons are independent.

Taking the SU(6) symmetry in the proton rest frame, we have

$$\Delta u^c = \frac{4}{3}, \quad \Delta d^c = -\frac{1}{3}. \quad (2.3.8)$$

From Eqs. (2.2.5) and (2.2.6) we know

$$\Delta u_v(\mu^2) = 0.644, \Delta d_v(\mu^2) = -0.348. \quad (2.3.9)$$

Using Eq. (2.3.7) we obtain

$$L_u^z(\mu^2) = 0.345, \quad L_d^z(\mu^2) = 0.007, \quad (2.3.10)$$

it implies that a polarized proton at scale μ^2 has two rotating u-quarks, while the d-quark is located at the center of the proton since it has almost zero-orbital momentum.

According to SU(6) symmetry, the constituent quark has zero angular momentum. However, according to Ref. [29,30,31,32] the orbital angular momentum $L_q^z(\mu^2)$ in Eq. (2.3.7) may origin from the transverse distribution of the constituent quark in the rest frame due to the Melosh-Wigner rotation [33]. The Melosh-Wigner rotation is a pure kinematic effect in the frame transformation, we consider that this effect should keep the angular momentum conservation, for say,

$$\frac{2}{3}\vec{s}_u^c = b\vec{s}_u + c\vec{L}_u, \quad (2.3.11)$$

where \vec{s}_u and \vec{L}_u are the spin and orbital angular momentum of a u-valence quark at μ^2 in the light-cone frame of the polarized proton; $2/3$ is from the SU(6)-distribution, the values of b and c depend on the wave function of valence quarks at μ^2 [29,30,31,32]. Because the spin is an elemental physical quantity, it is always has $|\vec{s}_u^c| = |\vec{s}_u| \equiv 1/2$, therefore, the orbital angular momentum \vec{L}_u changes only the direction of the spin from \vec{s}_u^c (it is also the polarized direction of the proton) to \vec{s}_u . Under these constraint conditions, once the values of b and c are determined by the wave function of valence quarks, the coupling angle between \vec{s}_u and \vec{L}_u in Eq. (2.3.11) can be fixed (see Fig. 12), and it leads to $\Delta u_v(\mu^2) < \Delta u^c$.

We discuss the evolution of the sum rule (2.3.2) with Q^2 . The evolution equation for the quark and gluon orbital angular momenta at the leading order approximation was derived by Ji, Tang and Hoodbhoy in [34], it reads

$$\begin{aligned}\frac{d\sum_q L_q^z(t)}{dt} &= \frac{\alpha_s(t)}{2\pi} \left[-\frac{4}{3} C_F \sum_q L_q^z(t) + \frac{n_f}{3} L_g^z(t) \right] + \frac{\alpha_s(t)}{2\pi} \left[-\frac{2}{3} C_F \Sigma(t) + \frac{n_f}{3} \Delta g(t) \right], \\ \frac{dL_g^z(t)}{dt} &= \frac{\alpha_s(t)}{2\pi} \left[\frac{4}{3} C_F \sum_q L_q^z(t) - \frac{n_f}{3} L_g^z(t) \right] + \frac{\alpha_s(t)}{2\pi} \left[-\frac{5}{6} C_F \Sigma(t) - \frac{11}{2} \Delta g(t) \right],\end{aligned}\quad (2.3.12)$$

where $C_F = 4/3$, n_f is the number of active quark flavors, $t = \ln(Q^2/\Lambda^2)$ and $t_0 = \ln(\mu^2/\Lambda^2)$. The solutions are

$$\sum_q L_q^z(Q^2) = -\frac{1}{2} \Delta \Sigma(Q^2) + \frac{1}{2} \frac{3n_f}{16 + 3n_f} + \left(\frac{t}{t_0}\right)^{-2(16+3n_f)/9\beta_0} \left[\sum_q L_q^z(\mu^2) + \frac{1}{2} \Delta \Sigma(\mu^2) - \frac{1}{2} \frac{3n_f}{16 + 3n_f} \right],$$

and

$$L_g^z(Q^2) = -\Delta g(Q^2) + \frac{1}{2} \frac{16}{16 + 3n_f} + \left(\frac{t}{t_0}\right)^{-2(16+3n_f)/9\beta_0} [L_g^z(\mu^2) + \Delta g(\mu^2) - \frac{1}{2} \frac{16}{16 + 3n_f}], \quad (2.3.13)$$

where $\beta_0 = 11 - 2n/3$. Because of $\Delta \Sigma(\mu^2) = 0.296$, $L_g^z(\mu^2) = 0$, $\Delta g(\mu^2) = 0$, we can fixed $\sum_q L_q^z(\mu^2) = 1/2 - \Delta \Sigma(\mu^2)/2 = 0.352$.

Table. The contributions of various components to the proton spin at different Q^2 .

Q^2	$0.064 GeV^2$	$1 GeV^2$	$10 GeV^2$	$100 GeV^2$
$\frac{1}{2} \Delta \Sigma$	0.148	0.149	0.151	0.153
$\sum_q L_q^z$	0.352	0.124	0.096	0.080
Δg	0	1.056	1.993	2.889
L_g^z	0	-0.829	-1.74	-2.622
Total	$\frac{1}{2}$	$\frac{1}{2}$	$\frac{1}{2}$	$\frac{1}{2}$

In Fig. 11 we add the curves of $\sum_q L_q^z(Q^2)$ and $L_g^z(Q^2)$ with $n_f = 3$. These results describe a following novel spin-orbital picture of the proton in the light-cone frame: The proton is mainly constructed by one d-valence quark and two u-valence quarks, the d-quark is located at the center of the proton, and the two u-quarks rotate with $\sum_q L_q^z(\mu^2) \simeq 0.35$ around the d-quark at a bound state scale, with the Q^2 increasing the valence quarks radiate gluons and then sea quarks follow them. The former builds fast rotating glue cloud (see Table), but their rotating direction is opposite to the u-quarks. Remind that the above mentioned possible orbital angular momentum of the partons in the polarized proton which can be checked in the experiments [35,36].

3 Spin structure function g_1^p at small x

3.1 A general consideration of the nucleon structure function at low Q^2

In the research of the nucleon structure functions at the full kinematic region, an argued question is whether the parton distributions and their perturbative QCD evolution can (even partly) be applied to the low Q^2 range or the parton concept is suddenly invalid at a critical value of $Q^2 \leq 1\text{GeV}^2$?

Let us begin from the parton model for the spin-dependent distribution, which is written based on the Collins-Soper-Sterman (CSS) factorization schema [37] at the collinear approximation and in the twist-2 level,

$$g_1(x, Q^2) = \int_0^1 \frac{dy}{y} \sum_q C_q(x/y, Q^2/\mu_F) \delta q(y, \mu_F), \quad (3.1.1)$$

which breaks up the spin structure function into two factors associated with perturbative short-distance functions C_a and nonperturbative polarized parton distributions δq at the factorization scale μ_F .

Taking the lowest order of C_q

$$C_q(x/y, Q^2/\mu_F) = \frac{1}{2} e_q^2 \delta(x/y - 1) \delta(Q - \mu_F) + \mathcal{O}(\alpha_s) + \mathcal{O}(1/Q), \quad (3.1.2)$$

$\mathcal{O}(\alpha_s)$ and $\mathcal{O}(1/Q)$ are the QCD radiative corrections and higher twist contributions. Inserting it to Eq. (3.1.1), we obtain the relation between the spin structure functions and the polarized quark distributions

$$g_1(x, Q^2) = \frac{1}{2} \sum_q e_q^2 [\delta q(x, Q^2) + \delta \bar{q}(x, Q^2)] + \mathcal{O}(\alpha_s) + \mathcal{O}(1/Q). \quad (3.1.3)$$

According to the renormalization group theory,

$$\frac{dg_1(x, Q^2)}{d \ln \mu_F} = 0, \quad (3.1.4)$$

it gives the DGLAP equation

$$Q^2 \frac{d}{dQ^2} \delta q(x, Q^2) = \int_0^1 \frac{dy}{y} \sum_{q'} \Delta P_{qq'}(x/y, \alpha_s(Q^2)) \delta q'(y, Q^2), \quad (3.1.5)$$

$\Delta P_{qq'}$ denotes the splitting functions. If we consider only the leading order (LO) approximation, we have

$$g_1^{DGLAP}(x, Q^2) = \frac{1}{2} \sum_q e_q^2 [\delta q(x, Q^2) + \delta \bar{q}(x, Q^2)], \quad (3.1.6)$$

These results are available at $Q^2 > \text{a few } GeV^2$.

At lower Q^2 , the multi-parton correlations are important and the inclusive lepton-nucleon cross section is dominated by complicate higher twist terms. In fact, according to the operator product expansion (OPE), the spin structure function in the proton $g_1^p(x, Q^2)$ can be expressed as a series in $1/Q^2$,

$$g_1^p(x, Q^2) = g_1^{LT}(x, Q^2) + g_1^{HT}(x, Q^2). \quad (3.1.7)$$

The leading (twist-2) term corresponds to scattering from a single free parton, while higher twist terms correspond to multi-parton interactions. Only a little of higher twist can be calculated perturbatively in terms of quark and gluon degrees of freedom. For example, the contributions of parton recombination at initial (or finite) state to the DGLAP evolution equation have been calculated at leading order [10,11,12,13] and we denote this result as $g_1^{DGLAP+ZRS}(x, Q^2)$. However, we can neither perform nor interpret a partonic calculation of the higher twist effects containing the correlations between the initial and finite partons since they break the factorization schema. In a certain kinematic regime, some of such higher twist contributions to $g_1^p(x, Q^2)$ appear as observable hadronic phenomenon. In this case, we may chose a suitable phenomenological model, even do a parametrization to describe the corresponding higher twist effects.

We try use the well known Vector Meson Dominance (VMD) model to mimic the above mentioned higher twist corrections. The reasons are as follows. The handbag diagram Fig.13a is a typical time ordered diagram describing Eq. (3.1.1), where the quark propagators connect with the probe and the target has only the forward components and these propagators can be broken as shown in Eq. (3.1.1) since they are on-mass-shell. The corresponding backward quark propagators construct the cat's ear diagram Fig.13b, which are neglected since these backward propagators are absorbed by the target in the collinear approximation [38,39]. However, the contributions of Fig. 13c can not been neglected at low Q^2 due to the corrections of quark-antiquark pair, which interacts with the target as a virtual vector meson if the transverse momentum $k_\perp \sim Q$ of quark pair is not large and confinement effects are essential. The contribution of Fig. 13c can not factorized as eq. (3.1.1). We use a phenomenological VMD model [40,41,42] to "isolate" this contribution from Fig. 13c. Traditionally, such VMD model was used to explain the structure function at low Q^2 region [43,44]. We denote this contribution as $g_1^{VMD}(x, Q^2)$.

The more complicated corrections to g_1 at low Q^2 are from the higher order QCD effects $\mathcal{O}(\alpha_f)$ and higher order recombination. In principle, we need to consider *all* these contributions, while it's beyond our ability. Our motivation is that if one finds empirically that higher order corrections are deduced with a suitable scale down to low $Q^2 (\sim \mu^2)$, then one can extend our leading order analysis of structure function data to μ^2 . If, the results are incompatible with the data, then the data can be used to extract the higher

order contributions.

In consequence, at lower Q^2 we have

$$g_1(x, Q^2) \simeq P g_1^{DGLAP+ZRS}(x, Q^2) + g_1^{VMD}(x, Q^2) + g_1^{HT}(x, Q^2), \quad (3.1.8)$$

where P is the probability of inelastic events via bare photon-parton interaction, the last term is the remaining higher twist corrections and we will neglect it at small x . Equation (3.1.8) implies that although the polarized partons share all nucleon's spin, the higher twist effects mix with the contributions of partons in the measuring spin structure function at low Q^2 . We emphasize that $g_1^{VMD}(x, Q^2)$ and $g_1^{HT}(x, Q^2)$ are irrelevant to the definition of the parton distributions because they violate the factorization schema, therefore, their contributions to $g_1(x, Q^2)$ will not change the discussions about spin in our previous section, which are the results of the polarized parton distributions in the proton.

3.2 Contributions of parton distributions and VMD part

The contributions of the polarized parton distributions of the proton to the spin structure functions at low Q^2 are

$$g_1^{DGLAP+ZRS}(x, Q^2) = \frac{1}{2} \sum_q e_q^2 [\delta q(x, Q^2) + \delta \bar{q}(x, Q^2)]. \quad (3.2.1)$$

We assume that all parton distributions are freezed at scale Q^2 if $Q^2 \leq \mu^2$. Based on this assumption we avoid the un-physical singularities at $Q \sim \Lambda_{QCD}$.

We present x -dependence of $g_1^{DGLAP+ZRS}(x, Q^2)$ at several values of Q^2 in Fig. 14. One can find the dramatic change of the spin structure function at $x < 10^{-3}$ from a flat form to dramatically decreasing. Considering Fig. 3, we conclude that the large gluon helicity effect leads to this phenomenon.

As we have mentioned that the contribution from the vector meson in virtual photon to g_1^p at $Q^2 < 1\text{GeV}^2$ is necessary. According to the VMD model [43,44],

$$xg_1^{VMD}(x, Q^2) = \frac{1}{8\pi} \frac{m_\rho^4 Q^2}{\gamma_\rho^2 (Q^2 + m_\rho^2)^2} \Delta\sigma_{pp}(s), \quad (3.2.2)$$

where γ_ρ is the coupling constant of ρ vector meson and proton; We consider the contributions of ρ meson since $\gamma_\rho \ll \gamma_\omega \ll \gamma_\phi$; x is a variable defined as $x = Q^2/(s + Q^2 - m_p^2)$ rather than a momentum fraction of parton, s is the CMS energy square of the γp collision. The cross-sections $\Delta\sigma_{pp}(s)$ is the total cross section for the scattering of polarized meson with the nucleon, unfortunately, they are unknown. Usually, the following Regge theory [45] is used,

$$\Delta\sigma_{pp}(s) \sim s^{\lambda-1}, \text{ at } s \rightarrow \infty. \quad (3.2.3)$$

The extrapolation of g_1^p from the measured region down to $x \sim 0$ suggests us to assume that $\lambda = 1 - \epsilon$ and $\epsilon \sim 0$ is a small positive parameter due to the requirement of integrability of g_1^p at $x \rightarrow 0$. In this work, we take $\epsilon = 0$. Thus, we have

$$g_1^{VMD}(x, Q^2) \simeq B \frac{m_\rho^2 Q^2}{(Q^2 + m_\rho^2)^2} x^{-1} (1-x)^7, \quad (3.2.4)$$

where $B = 0.03$ and the factor $(1-x)^7$ is due to the spectator counting rules at high x [46], and it restricts the application of the VMD model in small x range.

We read $m_\rho^4/(Q^2 + m_\rho^2)^2$ in Eq. (3.2.4) as the probability of the VMD event, therefore,

$$P = 1 - \frac{m_\rho^4}{(Q^2 + m_\rho^2)^2}, \quad (3.2.5)$$

in Eq.(3.1.8).

3.3 Predictions for spin structure function g_1^p at small x

What is the asymptotic behavior of g_1^p ? This is a broadly discussed subject. We plot $g_1^p(x, Q^2) = Pg_1^{DGLAP+ZRS}(x, Q^2) + g_1^{VMD}(x, Q^2)$ with different values of Q^2 in Fig. 15. There are two different asymptotic behaviors of g_1^p at small x : the VMD behavior $\sim x^{-1}$ at $Q^2 < 1\text{GeV}^2$ and the large gluon helicity effect at $Q^2 > 3\text{GeV}^2$. Besides, g_1^p presents the twist form of the two asymptotic behaviors above, which is the mixing result of the nonperturbative and perturbative dynamics.

We compare our predicted g_1^p at $x > 10^{-3}$ with the data [47] in Fig. 16. These data on 2010 are more precise than the previous data. Note that the values of Q^2 of every measured point are different and they are taken from Table I of [47]. The theoretical curve is a smooth connection among these points. This figure shows that the pQCD evolution almost control the behavior of g_1^p at $x > 10^{-3}$.

On the other hand, the combination of nonperturbative and perturbative dynamics at $x < 10^{-3}$ leads to a dramatic change of g_1^p around $Q^2 = 1 \sim 3\text{GeV}^2$. Unfortunately, there are only several data with large uncertainty about g_1^p in this range. In Figs. 17 and 18 we collect the HERA early data [48,49] at $Q^2 = 1, 10\text{GeV}^2$ which are un-generally used and compare them with our predicted g_1^p . Figure 19 shows some of these data (trigon) and the comparisons with our results (dark points). Figure 20 is the Q^2 -dependence of g_1^p with fixed x , the data are taken from [50]. One can find that our predicted g_1^p are compatible with these data, although more precise measurements are necessary.

Finally, we compare our results with the new COMAPSS (primary) data [14,15,16,17,18] at $Q^2 < 1\text{GeV}^2$, which show that g_1^p presents a flat asymptotic form at $x < 10^{-3}$. This seems to contradict with the predicted strong rise of g_1^p at $Q^2 < 1\text{GeV}^2$ in Fig.3. However, in the COMPASS fixed target experiments there is a strong correlation between x and Q^2 , which makes it possible that low x measurements are along with low Q^2 . In Fig. 21, we take the average values of Q^2 for each probing values of x (see Fig.1 in Ref.[15-18]). The results are acceptable. Obviously, the measurements at different x with different values of Q^2 in the fixed target experiments mix two different asymptotic behaviors of g_1^p .

We predict the stronger Q^2 - and x -dependence of g_1^p at $0.01 < Q^2 < 3\text{GeV}^2$ and $x < 0.1$ due to the mixture of nonperturbative vector meson interactions and the QCD evolution of the parton distributions in Fig.15. For testing this prediction, the measurements of g_1^p with fixed x or Q^2 at low Q^2 are necessary. The planning Electron-Ion Collider (EIC), for example, eRHIC [51] and EIC@HIAF [52] can probe a broad low $Q^2 < 1\text{GeV}^2$ -range, where we can check the predicted behavior of g_1^p at fixed x or Q^2 .

3.4 Discussions

In general consideration, both the logs of $1/x$ and Q^2 are equally important at small x and low Q^2 , and one should sum the double logarithmic (DL) terms $(\alpha_s \ln^2(1/x))^n$, which predict the singular behavior $g_1^p \sim x^{-\lambda}$ ($\lambda > 0$). It means that the BFKL equation [53,54,55,56,57,58] and its nonlinear corrections- the Balitsky-kovchegov equation [59,60,61] and the JIMWLK equation [62,63,64,65,66,67] should combine with the DGLAP equation. However, the translation between the BFKL equation and the DGLAP equation is a complicated technic. One of such method is the Ciafaloni-Catani-Fiorani-Marchesini (CCFM) equation [68,69,70,71], which is derived based on the two-scale unintegrated gluon distribution. The solution of the CCFM equation is much more complicated and has only proven to be practical with Monte Carlo generators. To avoid this difficulty, some special methods are proposed [72,73]. For example, the double logarithmic terms are taken into account via a suitable kernel of the evolution equations in the infrared evolution equations, which was first suggested by Lipatov [74,75], or alternatively taking a singular initial parton distributions at $x < 10^{-2}$, one can also mimic the results of the DL-resummation.

In this work, the behavior of g_1^p at the same range is obtained through a long evolution of the DGLAP equation with the parton recombination corrections. We find that it is different from the predictions of the DL-resummation, the asymptomatic behavior of the polarized quark distributions at $x \rightarrow 0$ is controlled by ΔP_{qg} in the DGLAP equation, rather than the $\ln^k(1/x)$ -corrections to the DGLAP-kernel. Thus, the difficult DL resummation can be replaced by the fits of the initial quark distributions $\delta q_v(x, \mu^2)$ in the DGLAP equation if the evolution distance is long enough. This conclusion was also obtained in the unpolarized structure functions [76].

4 Origins of the generalized Gerasimov-Drell-Hearn sum rule

4.1 Spin structure functions in the full Q^2 range

The Gerasimov-Drell-Hearn (GDH) sum rule reads

$$I_1(0) = \lim_{Q^2 \rightarrow 0} \frac{2M^2}{Q^2} \Gamma_1(Q^2) = -\frac{\kappa^2}{4} \sim -0.8, \quad (4.1.1)$$

where κ is the anomalous magnetic moment of the nucleon. On the other hand, the Bjorken sum rule [77] says

$$\lim_{Q^2 \rightarrow \infty} [\Gamma_1^p(Q^2) - \Gamma_1^n(Q^2)] = \frac{1}{6} \left| \frac{g_A}{g_V} \right|, \quad (4.1.2)$$

this ratio is accurately known as[78]: $g_A/g_V = -1.2695 \pm 0.0029$.

The connection of the two sum rules by means of the generalized GDH sum rule is (For an overview, see Ref. [79] for example)

$$I_1(Q^2) = \frac{2M^2}{Q^2} \Gamma_1(Q^2), \quad (4.1.3)$$

which allows us to study the transition between the perturbative partonic structure and nonperturbative hadronic picture of nucleon in lepton-nucleon scattering processes. The data show that this sum rule at low $Q^2 < 1 \text{ GeV}^2$ changes dramatically and exceeds the variation bound at higher Q^2 , which has been parameterized (but not explanation) in [80,81,82,83]. The explanation of the generalized GDH sum rule is an active subject. For example, the phenomenological constituent quark model [84,85], the VMD model [86,87], the resonance contributions [88], the chiral perturbation theory (χ PT) [89,90,91] are used to understand the generalized GDH sum rule.

The first moment of g_1^p is

$$\Gamma_1^p(Q^2) = \Gamma_1^{DGLAP+ZRS}(Q^2) + \Gamma_1^{VMD}(Q^2) + \Gamma_1^{HT}(Q^2). \quad (4.1.4)$$

From Eqs. (3.1.8) and (3.2.5) we obtain

$$\Gamma_1^{DGLAP+ZRS}(Q^2) \simeq 0.123 \left(1 - \frac{m_v^4}{(Q^2 + m_v^2)^2} \right). \quad (4.1.5)$$

The dashed curve in Fig. 22 is our predicted $\Gamma_1^{DGLAP+ZRS}(Q^2)$. On the other hand, we have

$$\Gamma_1^{VMD}(Q^2) = \int_0^1 dx g_1^{VMD}(x, Q^2) \simeq 0.055 \frac{m_v^2 Q^2}{(Q^2 + m_v^2)^2}. \quad (4.1.6)$$

Comparing the solid curve with $\Gamma_1^p(Q^2)$ data [92,93,94,95,96,97,98] in Fig. 22, one can expect that the remaining higher twist corrections g_1^{HT} play a significant role at low Q^2 to the general GDH sum rule. We will discuss them in detail next section.

4.2 Higher twist contributions to the GDH sum rule

According to the OPE, the appearance of scaling violations at low Q^2 is related to the higher twist corrections to moments of structure functions. Higher twists are expressed as matrix elements of operators involving nonperturbative interactions between quarks and gluons. The study of higher twist corrections gives us a direct insight into the nature of long-range quark-gluon correlations. The higher twist corrections to g_1 have several representations. In this work, we will try to expose the remaining power suppression corrections to Γ_1^p . For this sake, we make $\Gamma_1^{HT}(Q^2)$ (i.e., the data points in Fig. 22)- $[\Gamma_1^{DGLAP+ZRS}(Q^2) + \Gamma_1^{VMD}(Q^2)]$. Figure 23 shows such a result at $Q^2 > 0.2 \text{ GeV}^2$, which has been smoothed with minimum $\chi^2/D.o.f.$.

To expose the possible physical information of the curve in Fig. 23, according to QCD operator product $1/Q^2$ -expansion,

$$\Gamma_1^{HT}(Q^2) = \sum_{i=2}^{\infty} \frac{\mu_{2i}(Q^2)}{Q^{2i-2}}, \quad (4.2.1)$$

we take first three approximations

$$\Gamma_1^{HT(4)}(Q^2) = \frac{\mu_4(Q^2)}{Q^2}, \quad (4.2.2)$$

$$\Gamma_1^{HT(4+6)}(Q^2) = \frac{\mu_6(Q^2) + \mu_4(Q^2)Q^2}{Q^4}, \quad (4.2.3)$$

$$\Gamma_1^{HT(4+6+8)}(Q^2) = \frac{\mu_8(Q^2) + \mu_6(Q^2)Q^2 + \mu_4(Q^2)Q^4}{Q^6}. \quad (4.2.4)$$

Then we plot the curves $Q^2\Gamma_1^{HT(4)}(Q^2)$, $Q^4\Gamma_1^{HT(4+6)}(Q^2)$ and $Q^6\Gamma_1^{HT(4+6+8)}(Q^2)$ in Fig. 24. There are following interesting properties of these results:

(i) $Q^6\Gamma_1^{HT(4+6+8)}(Q^2) \rightarrow 0$, if $Q^2 \rightarrow 0$. This implies that μ_8 vanishes if it is independent of Q^2 . Therefore, $\Gamma_1^{HT(4+6)}(Q^2)$ is an appropriate approximation.

(ii) Three curves in Fig. 24 cross at a same point $Q^2 \sim 1 \text{ GeV}^2$. Particularly, the intercept μ_6 of the line suddenly changes its value from -0.037 at $Q^2 > 1 \text{ GeV}^2$ to 0.006 at $Q^2 < 1 \text{ GeV}^2$. This result exposes that the correlation among partons in the proton has an obvious change near $Q \sim 1 \text{ GeV}$.

(iii) We use

$$\Gamma_1^{HT(4+6)}(Q^2) = \frac{\mu_4}{Q^2 + \epsilon^2} + \frac{\mu_6}{(Q^2 + \epsilon^2)^2} \quad \text{at } Q^2 < 0.3 \text{ GeV}^2 \quad (4.2.5)$$

to fit the data at $Q^2 < 0.3 \text{ GeV}^2$, where we add a parameter ϵ to remove the unnatural singularity at $Q^2 = 0$. The value of ϵ is sensitive to $I(0)$. We find that $\mu_4 = -0.13 \text{ GeV}^2$, $\mu_6 = 0.0528 \text{ GeV}^4$ and $\epsilon^2 = 0.422 \text{ GeV}^2$.

In summary,

$$\Gamma_1^p(Q^2) = 0.123 \left(1 - \frac{m_v^4}{(Q^2 + m_v^2)^2} \right) + 0.055 \frac{m_v^2 Q^2}{(Q^2 + m_v^2)^2} + \Gamma_1^{HT}(Q^2) \quad (4.2.6)$$

where the HT contributions are

$$\Gamma_1^{HT}(Q^2) = \begin{cases} \frac{0.004M^2}{Q^2} - \frac{0.037M^4}{Q^4} & \text{at } Q^2 > 1GeV^2 \\ -\frac{0.048M^2}{Q^2} + \frac{0.0073M^4}{Q^4} & \text{at } 0.3 < Q^2 < 1GeV^2 \\ -\frac{0.13M^2}{Q^2+0.422M^2} + \frac{0.0528M^4}{(Q^2+0.422M^2)^2} & \text{at } Q^2 < 0.3 GeV^2 \end{cases}, \quad (4.2.7)$$

where $M^2 = 1GeV^2$. We present the comparison of our $\Gamma_1^p(Q^2)$ with the data [92,93,94,95,96,97,98] in Fig. 25. The corresponding $I_1^p(Q^2)$ is presented in Fig. 26.

4.3 Discussions

The parton-hadron duality was first noted by Bloom and Gilman [99,100] in deep inelastic scattering (DIS) and has been confirmed by many measurements. At low energies (or intermediate Bjorken variable x and low Q^2) DIS reactions are characterized by excitation of nucleon resonances; while at high virtuality such processes have a partonic description. The smooth high-energy scaling curve essentially reproduces the average of the resonance peaks seen at low energies. Burkert and Ioffe [81] indicated that the contribution of the isobar $\Delta(1232)$ electro-production at small Q^2 can describe the general GDH sum rule, and they gave

$$\frac{\mu_4}{M^2} = -0.056 \sim -0.063, \text{ at } Q^2 = 0.3 \sim 0.8 \text{ GeV}^2 \quad (4.3.1)$$

$$\frac{\mu_6}{M^4} = 0.010 \sim 0.011, \text{ at } Q^2 = 0.3 \sim 0.8 \text{ GeV}^2, \quad (4.3.2)$$

which are compatible with our prediction Eq. (4.2.7).

Our results in Fig.24 indicate that the negative twist-6 and twist-4 effects dominate the suppression of $\Gamma_1^p(Q^2)$ at $Q^2 > 1\text{GeV}^2$ and $Q^2 < 1\text{GeV}^2$. Particularly, the slope of μ_4 of the lines, which cuts $Q^4\Gamma_1^{HT(4+6)}(Q^2)$ suddenly changes its sign at $Q^2 < 1 \text{ GeV}^2$. This result exposes that the correlation among partons in the proton become stronger at scale $\sim 0.2 \text{ fm}$. We noted that Petronzio1, Simula and Ricco [101] reported that the inelastic proton data obtained at Jefferson Lab exhibit a possible extended objects with size of $\simeq 0.2 - 0.3 \text{ fm}$ inside the proton.

5 Summary

In this work we consider that the nucleon is consisted of quarks and gluons (partons) via QCD interactions even at low Q^2 . A general worry is that the correlations among partons may break the definition of parton distributions and their evolution rules. As a model, we treat these high twist effects as two parts: (i) The leading recombination among initial partons, which modifies the DGLAP equation but keeps the momentum conservation in Eqs. (2.2.1)-(2.2.3) and the nucleon helicity sum rule Eq. (2.3.2); (ii) The phenomenological VMD model and the parameterized higher twist effects, which contribute to the measured structure functions of the nucleon but they are irrelevant to the parton distributions in the nucleon. In this framework, we discuss the electron scattering off a nucleon at high energy in a special (Bjorken) infinite momentum frame, where the virtual photon presents two components: bare photon γ^* and vector meson V^* with $J^{PG} = 1^{--}$. In the former case, γ^* couples either with an on-mass-shell quark and contributes $F_2^{DGLAP+ZRS}$, where we take a leading order approximation and all higher order corrections are absorbed into the free parameters, or with an off-mass-shell quark, which gives F_2^{HT} . In the later case, the VMD model describes the nonperturbative multi-parton interactions between V^* and nucleon. Thus, we present a compact theoretical model about the nucleon spin structure.

(i) We find that the gluon contribution to the spin of proton is much larger than the predictions of most other theories. This result is compatible with the recent NNPDF analysis and suggests a significant orbital angular momentum of gluons to balance the contribution of gluon spin. In concretely, the total proton spin at a bound state scale μ^2 is composed by $\sim 30\%$ quark spin and $\sim 70\%$ orbital angular momentum of the quarks, where two u-valence quarks are rotating around a d-valence quark. With increasing Q^2 , the omitted gluons accumulate a larger positive helicity, which is mainly balanced by their orbital momentum. Therefore, there are two rotating groups in a polarized proton at Q^2 : a slower quark group and a faster gluon.

(ii) We use the DGLAP equation with the parton recombination corrections and the nonperturbative VMD model to predict the spin structure functions g_1^p of the proton. We first present a complete picture for the translation of g_1^p from low Q^2 (~ 0) to high Q^2 at small x . We find that the contribution of the large gluon helicity dominates g_1^p at $x > 10^{-3}$, but the mixture with nonperturbative component complicates the asymptomatic behavior of g_1^p at $x < 10^{-3}$. The results are compatible with the data including the early HERA estimations and COMPASS new results. The predicted strong Q^2 - and x -dependence of g_1^p at $0.01 < Q^2 < 3\text{GeV}^2$ and $x < 0.1$ due to the mixture of nonperturbative vector meson interactions and the QCD evolution of the parton distributions can be checked on the next Electron-Ion Collider (EIC).

(iii) We discuss the contributions of parton distributions and VMD component to the

lowest moment of the spin-dependent proton structure function. After removing the above two contributions from the existing experimental data for $\Gamma_1^p(Q^2)$, the higher twist power corrections present their interesting characters: parton correlations at $Q^2 \sim 1 \text{ GeV}^2$ show a bend point, where the twist-4 and twist-6 effects dominate the suppression of $\Gamma_1^p(Q^2)$ at $Q^2 < 1 \text{ GeV}^2$ and $Q^2 > 1 \text{ GeV}^2$, respectively. The results suggest a possible extended objects with size $0.2 - 0.3 \text{ fm}$ inside the proton. Within the analytic of these results, we are able to achieve a rather good description of the data at all Q^2 region using a simple parameterized form of $\Gamma_1^p(Q^2)$.

Appendix:

From Ref.[13], we have LO polarized gluon recombination functions

$$P_{g+g+\rightarrow g+} = \frac{9}{4} \frac{(x_1 + x_2 - x)^3}{xx_2^2(x_1 + x_2)^3 x_1^2} (x_1^4 - 2x_1^3x + x_1^2x^2 + x_2^4 - 2x_2^3x + x_2^2x^2 + x_1^2x_2^2 - x_1^2x_2x - x_1x_2^2x + x_1x_2x^2) \quad (\text{A.1})$$

$$P_{g+g+\rightarrow g-} = \frac{9}{4} \frac{(x_1 + x_2 - x)}{xx_2^2(x_1 + x_2)^3 x_1^2} (6x_1^4x_2x + 6x_1^3x_2^2x - 3x_1^3x_2x^2 - 7x_1^2x_2x^3 + 11x_1^2x_2^2x^2 + 6x_2^4x_1x + 6x_2^3x_1^2x - 3x_2^3x_1x^2 - 7x_2^2x_1x^3 + 2x_1x_2x^4 + x_1^6 + x_2^6 + 2x_1^5x_2 + 2x_1^4x_2^2 - x_1^4x^2 - 2x_1^3x^3 + 2x_1^2x^4 + 2x_2^5x_1 + 2x_2^4x_1^2 - x_2^4x^2 - 2x_2^3x^3 + 2x_2^2x^4 + 2x_1^3x_2^3) \quad (\text{A.2})$$

$$P_{g+g-\rightarrow g+} = \frac{9}{4} \frac{(x_1 + x_2 - x)}{xx_2^2(x_1 + x_2)^7 x_1^2} (141x_1^7x^2x_2 + 42x_1^4x^4x_2^2 - 100x_1^8xx_2 + 19x_1^5x^4x_2 - 5x_2^8x_1x + 39x_1^2x^4x_2^4 + 137x_1^3x_2^6x - 86x_1^6x^3x_2 + 26x_2^9x_1 + 5x_1^{10} + 5x_2^{10} + 155x_1^4x^2x_2^4 - 40x_1^2x_2^5x^3 - 212x_1^6xx_2^3 - 124x_1^3x^3x_2^4 - 196x_1^4x^3x_2^3 - 79x_1^2x_2^6x^2 + 128x_1^4x_2^5x + 44x_2^7x_1^2x - 47x_1^5xx_2^4 - 177x_1^5x^3x_2^2 - 209x_1^7xx_2^2 + 40x_1^3x^4x_2^3 - 33x_1^3x_2^5x^2 + x_2^6x_1x^3 + 319x_1^5x^2x_2^3 + 291x_1^6x^2x_2^2 - 35x_2^7x_1x^2 + 13x_2^5x^4x_1 + 64x_2^7x_1^3 + 57x_2^8x_1^2 + 26x_1^9x_2 + 57x_1^8x_2^2 + 64x_1^7x_2^3 + 34x_1^6x_2^4 + 12x_1^5x_2^5 + 34x_1^4x_2^6 - 4x_2^9x + 2x_2^6x^4 + 2x_2^7x^3 - 5x_2^8x^2 + 30x_1^8x^2 - 20x_1^7x^3 + 5x_1^6x^4 - 20x_1^9x) \quad (\text{A.3})$$

$$P_{g+g-\rightarrow g-} = \frac{9}{4} \frac{(x_1 + x_2 - x)}{xx_2^2(x_1 + x_2)^7 x_1^2} (-31x_1^7x^2x_2 + 27x_1^4x^4x_2^2 - 7x_1^8xx_2 + 9x_1^5x^4x_2 - 104x_2^8x_1x + 54x_1^2x^4x_2^4 - 206x_1^3x_2^6x + 3x_1^6x^3x_2 + 26x_2^9x_1 + 5x_1^{10} + 5x_2^{10} + 115x_1^4x^2x_2^4 - 211x_1^2x_2^5x^3 + 125x_1^6xx_2^3 - 192x_1^3x^3x_2^4 - 92x_1^4x^3x_2^3 + 319x_1^2x_2^6x^2 - 25x_1^4x_2^5x - 217x_2^7x_1^2x + 136x_1^5xx_2^4 - 24x_1^5x^3x_2^2 + 34x_1^7xx_2^2 + 36x_1^3x^4x_2^3 + 307x_1^3x_2^5x^2 - 106x_2^6x_1x^3 - 41x_1^5x^2x_2^3 - 67x_1^6x^2x_2^2 + 157x_2^7x_1x^2 + 27x_2^5x^4x_1 + 64x_2^7x_1^3 + 57x_2^8x_1^2 + 26x_1^9x_2 + 57x_1^8x_2^2 + 64x_1^7x_2^3 + 34x_1^6x_2^4 + 12x_1^5x_2^5 + 34x_1^4x_2^6 - 20x_2^9x + 5x_2^6x^4 - 20x_2^7x^3 + 30x_2^8x^2 - 5x_1^8x^2 + 2x_1^7x^3 + 2x_1^6x^4 - 4x_1^9x) \quad (\text{A.4})$$

Setting $x_1 = x_2 = y$, one can find

$$\Delta P_{gg \rightarrow g} = [P_{g+g+\rightarrow g+} - P_{g+g+\rightarrow g-} - P_{g+g-\rightarrow g+} + P_{g+g-\rightarrow g-}]$$

$$\begin{aligned}
&= [P_{g+g+\rightarrow g+} - P_{g+g+\rightarrow g-} + P_{g+g-\rightarrow g+} - P_{g+g-\rightarrow g-}] \\
&= \frac{27(2y-x)(-20y^3+12y^2x-x^3)}{64y^5}
\end{aligned}$$

Similarly,

$$\begin{aligned}
P_{g+g+\rightarrow q+} &= \frac{1}{12} \frac{(x_1+x_2-x)^2}{(x_1+x_2)^3 x_2^2 x_1^2} (4x_1^4 + 7x_1^3 x_2 - 8x_1^3 x + 2x_1^2 x_2^2 - 6x_1^2 x x_2 \\
&\quad + 4x^2 x_1^2 + 4x^2 x_2^2 - x_1 x_2^3 + 2x_1 x x_2^2 - x_1 x_2 x^2) \quad (A.5)
\end{aligned}$$

$$\begin{aligned}
P_{g+g+\rightarrow q-} &= \frac{1}{12} \frac{(x_1+x_2-x)^2}{(x_1+x_2)^3 x_2^2 x_1^2} (4x^2 x_1^2 + 4x_1^2 x_2^2 + 8x_1 x_2^3 - 8x_1 x x_2^2 + 4x_2^4 \\
&\quad - 8x_2^3 x + 4x^2 x_2^2 - x_1 x_2 x^2) \quad (A.6)
\end{aligned}$$

$$\begin{aligned}
P_{g+g-\rightarrow q+} &= \frac{1}{12} \frac{(x_1+x_2-x)^2}{(x_1+x_2)^7 x_2^2 x_1^2} (4x_1^6 x^2 + 4x_1^4 x_2^4 - 8x_1^7 x + 24x_1^6 x_2^2 + 16x_1^5 x_2^3 \\
&\quad + 16x_1^7 x_2 + 4x_1^8 + 24x^2 x_2^5 x_1 + 4x^2 x_2^6 - 10x_1^3 x^2 x_2^3 + 33x_1^2 x^2 x_2^4 \\
&\quad - 8x_1^4 x x_2^3 + 24x_1^5 x^2 x_2 + 33x_1^4 x^2 x_2^2 + 14x_1^3 x x_2^4 - 40x_1^6 x x_2 \\
&\quad - 53x_1^5 x x_2^2 - 8x x_2^5 x_1^2 - 9x_1 x x_2^6) \quad (A.7)
\end{aligned}$$

$$\begin{aligned}
P_{g+g-\rightarrow q-} &= \frac{1}{12} \frac{(x_1+x_2-x)^2}{(x_1+x_2)^7 x_2^2 x_1^2} (24x_2^6 x_1^2 + 16x_2^7 x_1 - 8x_2^7 x + 16x_2^5 x_1^3 + 4x_2^8 \\
&\quad + 4x_1^6 x^2 + 4x_1^4 x_2^4 + 6x^2 x_2^5 x_1 + 4x^2 x_2^6 + 8x_1^3 x^2 x_2^3 + 15x_1^2 x^2 x_2^4 \\
&\quad - 13x_1^4 x x_2^3 + 24x_1^5 x^2 x_2 + 51x_1^4 x^2 x_2^2 - 35x_1^3 x x_2^4 + x_1^5 x x_2^2 \\
&\quad - 35x x_2^5 x_1^2 - 22x_1 x x_2^6) \quad (A.8)
\end{aligned}$$

Setting $x_1 = x_2 = y$, we have

$$\begin{aligned}
\Delta P_{gg \rightarrow q} &= [P_{g+g+\rightarrow q+} - P_{g+g+\rightarrow q-} - P_{g+g-\rightarrow q+} + P_{g+g-\rightarrow q-}] \\
&= [P_{g+g+\rightarrow q+} - P_{g+g+\rightarrow q-} + P_{g+g-\rightarrow q+} - P_{g+g-\rightarrow q-}] \\
&= \frac{1}{48} \frac{(2y-x)^2(-y+x)}{y^4}
\end{aligned}$$

References

- [1] NNPDF Collaboration, E. R. Nocera, R. D. Ball, S. Forte, G. Ridolfi and J. Rojo, to be published in Nucl.Phys. B, hep-ph/ 1406.5539.
- [2] G. Parisi and R. Petronzio, Phys. Lett. **B62**, 331 (1976).
- [3] V.A. Novikov, M.A. Shifman, A.I. Vainshtein, V.I. Zakharov, JETP Lett., **24**, 341 (1976).
- [4] M. Glück, E. Reya, Nucl.Phys. **B130**, 76 (1977).
- [5] X.R. Chen, J.H. Ruan, R. Wang, P.M. Zhang and W. Zhu, Int. J. Mod. Phys. **E23**, 14500057 (2014), hep-ph/1306.1872.
- [6] X.R. Chen, J.H. Ruan, R. Wang, P.M. Zhang and W. Zhu, **E23**, 1450058 (2014), hep-ph/1306.1874.
- [7] G. Altarelli, G. Parisi, Nucl. Phys. **B126**, 298 (1977).
- [8] V.N. Gribov, L.N. Lipatov, Sov. J. Nucl. Phys. **15**, 438 (1972).
- [9] Yu.L. Dokshitzer, Sov. Phys. JETP **46**, 641 (1977).
- [10] W. Zhu, Nucl. Phys. **B551**, 245 (1999), hep-ph/9809391;
- [11] W. Zhu, J.H. Ruan, Nucl. Phys. **B559**, 378 (1999), hep-ph/9907330v2.
- [12] W. Zhu and Z.Q. Shen, HEP & NP, **29**, 109 (2005), hep-ph/0406213v3.
- [13] W. Zhu, Z.Q. Shen and J.H. Ruan, Nucl.Phys. **B692**, 417 (2004), hep-ph/0406212v2[hep-ph].
- [14] A.S. Nunes (on behalf of the COMPASS Collab.,) Longitudinal double spin asymmetry A_1^p and spin-dependent structure function g_1^p of the proton at low x and low Q^2 from COMPASS, Proceedings of the XV workshop on high energy spin physics, Dubna, Russia, (2013), hep-ex/1405.5811.
- [15] COMPASS Collaboration, P. Abbon et al., Nucl. Instr. and Meth. **A577**, 455 (2007).
- [16] E.S. Ageev et al., Phys. Lett. **B612**, 154 (2005).
- [17] V.Yu. Alexakhin et al., Phys. Lett. **B647**, 8 (2007).
- [18] M.G. Alekseev et al., Phys. Lett. **B690**, 466 (2010).

- [19] S.B. Gerasimov, Sov. J. Nucl. Phys. **2**, 430 (1966).
- [20] S.D. Drell and A.C. Hearn, Phys. Rev. Lett. **16**, 908 (1966).
- [21] NM Collaboration, J. Ashman et al., Nucl. Phys. **B328**, 1 (1989) and references therein.
- [22] M. Glück, E. Reya, and A. Vogt, Eur. Phys. J. **C5**, 461 (1998)..
- [23] COMPASS Collaboration, C. Adolph, et. al., hep-ex/1202.4064.
- [24] D. de Florian, R. Sassot, M. Stratmann and W. Vogelsang, Phys. Rev. Lett. **113**, 012001 (2014), hep-ph/1404.4293.
- [25] P. Djawotho for the STAR Collaboration, nucl-ex/1303.0543.
- [26] PHENIX Collaboration, A. Adare et al., Phys. Rev. **D90**, 012007 (2014), hep-ex/1402.6296.
- [27] J. Ellis and M. Karliner, Phys. Lett., **B341**, 397 (1995).
- [28] A. Airapetian, et.al., Phys, Pev. **D75**, 012007 (2007).
- [29] B.Q. Ma, J. Phys, **G17**, L53 (1991).
- [30] B.Q. Ma and S.J. Brodsky, The spin and flavor content of intrinsic sea quarks, hep-ph/9707408.
- [31] B.Q. Ma, I. Schmidt and J. Soffer, Phys. Lett. **B441**, 461 (1998).
- [32] B.Q. Ma and I. Schmit, Phys. Rev. **D58** 096008 (1998).
- [33] H.J. Melosh, Phys. Rev. **D9**, 1095 (1974); E. Wigner, Ann. Math. **40**, 149 (1939).
- [34] X.D. Ji, J. Tang and P. Hoodbhoy, Phys. Rev. Lett.**76**, 740 (1996).
- [35] T.C. Meng, J.C. Pan, Q.B. Xie and W. Zhu, Phys. Rev. **D40**, 769 (1989).
- [36] T.C. Meng, Invited talk given at the Workshop on the Prospects of Spin Physics at HERA, DESY Zeuthen, August 28-31, 1995 hep-ph/9510336.
- [37] J.C. Collins, D.E. Soper, G. Sterman, in: A.H. Mueller (Ed.), Perturbative Quantum Chromodynamics, World Scientific, Singapore, 1989, p. 1.
- [38] W. Zhu, H.W. Xiong, J.H. Ruan, Phys. Rev. **D60**, 094006 (1999).
- [39] W. Zhu, Nucl. Phys. **A753**, 206 (2005).

- [40] J.J. Sakurai, currents and mesons, university of Chigag, Chigago (1969).
- [41] T. H. Bauer et al., Rev. Mod. Phys. **50**, 261 (1978).
- [42] G. Grammer Jr and J. D. Sullivan, in Electromagnetic Interactions of Hadrons, edited by A. Donnachie and G. Shaw, Plenum, New York, 1978, Vol.2.
- [43] B. Badelek, J. Kwieciski, B. Ziaja, Eur. Phys. J. **C26**, 45 (2002).
- [44] B. Badelek, J. Kwieciski, B. Ziaja, Acta Phys. Polon. **B33**, 3701 (2002).
- [45] P.D.B. Collins, An Introduction to Regge Theory and High Energy Physics, Cambridge University Press, Cambridge, 1977.
- [46] S.J. Brodsky and G. Farrar, Phys. Rev. Lett. **31**, 1153 (1973).
- [47] COMPASS Collaboration, M.G. Alekseev, et al Phys. Lett. **B690**, 466 (2010).
- [48] R. D. Ball, A. Deshpande, S. Forte, V. W. Hughes, J. Lichtenstadt,, G. Ridolf, Measurement of the polarized sreucture function $g_1^p(x, Q^2)$ at HERA, hep-ph/9609515.
- [49] J. Kwiecinski and B. Ziaja, hep-ph/9802386.
- [50] A. De Roeck, A. Deshpande, V.W. Hughes, J. Lichtenstadt, G. Radcl Eur. Phys. J. **C6**, 121 (1999).
- [51] E.C. Aschenauer, at. al., eRHIC Design Study: An Electron-Ion Collider at BNL, hep-ph/1409.1633.
- [52] X.R. Chen, An Electro Ion Collider Plan in China, Invited talk at the 21st International Symposium on Spin Physics, Beijing, China, Oct. 20-24 (2014).
- [53] L.N. Lipatov, Sov. J. Nucl. Phys. **23**, 338 (1976).
- [54] V.S. Fadin, E.A. Kuraev, L.N. Lipatov, Phys. Lett. **B60**, 50 (1975).
- [55] E.A. Kuraev, L.N. Lipatov, V.S. Fadin, Sov. Phys. JETP **44**, 443 (1976).
- [56] E.A. Kuraev, L.N. Lipatov, V.S. Fadin, Sov. Phys. JETP **45**, 199 (1977).
- [57] I.I. Balitsky, L.N. Lipatov, Sov. J. Nucl. Phys. **28**, 822 (1978).
- [58] I.I. Balitsky, L.N. Lipatov, JETP Lett. **30**, 355 (1979) .
- [59] I. Balitsky, Nucl. Phys. **B463** (1996) 99.
- [60] Yu. Kovchegov, Phys. Rev. **D60** (1999) 034008.

- [61] Yu. Kovchegov, Phys. Rev. **D61** (2000) 074018.
- [62] J. Jalilian-Marian, A. Kovner, L. McLerran, and H. Weigert, Phys. Rev. **D55**, 5414 (1997).
- [63] J. Jalilian-Marian, A. Kovner, A. Leonidov, and H. Weigert, Nucl. Phys. **B504**, 415 (1997).
- [64] J. Jalilian-Marian, A. Kovner, A. Leonidov, and H. Weigert, Phys. Rev. **D59**, 014014 (1998).
- [65] H. Weigert, Nucl. Phys. **A703**, 823 (2002).
- [66] E. Iancu, A. Leonidiv, and L. McLerran, ibid. **A692**, 583 (2001).
- [67] E. Iancu, A. Leonidiv, and L. McLerran, Phys. Lett. **B510**, 133 (2001).
- [68] M. Ciafaloni, Nucl. Phys. **B296**, 49 (1988).
- [69] S. Catani, F. Fiorani, and G. Marchesini, Phys. Lett. **B234**, 339 (1990).
- [70] S. Catani, F. Fiorani, and G. Marchesini, Nucl. Phys. **B336**, 18 (1990).
- [71] G. Marchesini, Nucl. Phys. **B445**, 49 (1995).
- [72] D. Kotlorz and A. Kotlorz, Acta Phys. Polon. **B39**, 1913 (2008).
- [73] B.I. Ermolaev, M. Greco, S.I. Troyan, Riv. Nuovo Cim. **33**, 57 (2010).
- [74] L.N. Lipatov, Zh. Eksp. Teor. Fiz. **82**, 991 (1982).
- [75] L.N. Lipatov, Phys. Lett. **B116**, 411 (1982).
- [76] M. Glück, E. Reya, and A. Vogt, Eur. Phys. J. **C5**, 461 (1998).
- [77] J.D. Bjorken, Phys. Rev. **148**, 1467 (1966).
- [78] Particle Data Group, S. Eidelman et al., Phys. Lett. **B592**, 1 (2004).
- [79] D. Drechsel, S.S. Kamalov and L. Tiator, Phys. Rev. **D63**, 114010 (2001) hep-ph/0008306.
- [80] M. Anselmino, B.L. Ioffe and E. Leader, 1989, Sov. J. Nucl. Phys. **49**, 136 (1989).
- [81] V.D. Burkert and B.L. Ioffe, Phys. Lett. **B296**, 223 (1992).
- [82] J. Soffer and O.V. Teryaev, Phys. Rev. Lett. **70**, 3373 (1993).

- [83] J. Soffer and O. Teryaev, Phys. Rev. **D70**, 116004 (2004).
- [84] D. Drechsel and L. Tiator Ann. Rev. Nucl. Part. Sci. **54**, 69 (2004), nucl-th/0406059.
- [85] M. Gorchtein, D. Drechsel, M.M. Giannini, E. Santopinto and L. Tiator, Phys. Rev. **C70**, 055202 (2004) 055202, hep-ph/0404053.
- [86] B. Badelek, J. Kiriyluk, and J. Kwiecinski Phys. Rev. **D61**, 014009, hep-ph/9907569.
- [87] B. Badelek, J. Kwiecinski and B. Ziaja, Eur. Phys. J. **C26**, 45 (2002), hep-ph/0206188.
- [88] D. Burkert and Z.J. Li, Phys. Rev. **D47**, 46 (1993).
- [89] V. Bernard, Prog. Part. Nucl. Phys. **60**, 82 (2006).
- [90] V. Bernard et al., Phys. Rev. **D67**, 076008 (2003).
- [91] X. Ji et al., Phys. Lett. **B472**, 1 (2000).
- [92] HERMES Collaboration, A. Airapetian et al., Eur. Phys. J. **C26** (2003) 527, hep-ex/0210047.
- [93] HERMES Collaboration, A. Airapetian et al., Phys. Rev., **D75**, 012007 (2007).
- [94] E143 Collaboration, K. Abe et al., Phys. Rev. Lett. **78**, 815 (1997), hep-ex/9701004.
- [95] CLAS Collaboration, R. Fatemi et al., Phys. Rev. Lett. **91**, 222002 (2003), nucl-ex/0306019.
- [96] K. V. Dharmawardane et al., Phys. Lett. **B641**, 11 (2006).
- [97] P. E. Bosted et al., Phys. Rev. **C75**, 035203 (2007).
- [98] Y. Prok et al., Phys. Lett. **B672**, 12 (2009).
- [99] E.D. Bloom and E.J. Gilman, Phys. Rev. Lett. **25**, 1140 (1970).
- [100] E.D. Bloom and E.J. Gilman, Phys. Rev. **D4**, 2901 (1971).
- [101] R. Petronzio, S. Simula, G. Ricco, Phys. Rev. **D67**, 094004 (2003), hep-ph/0301206.

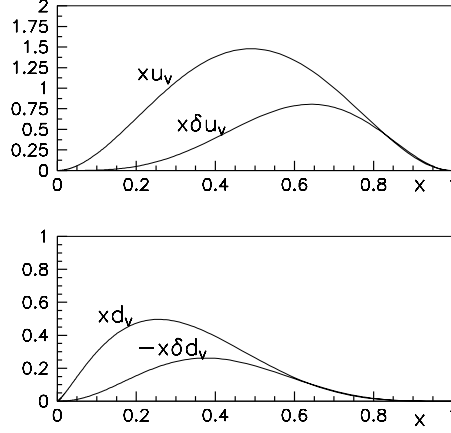


Figure 1: Input valence quark distributions at $\mu^2 = 0.064 GeV^2$ for polarized and unpolarized densities.

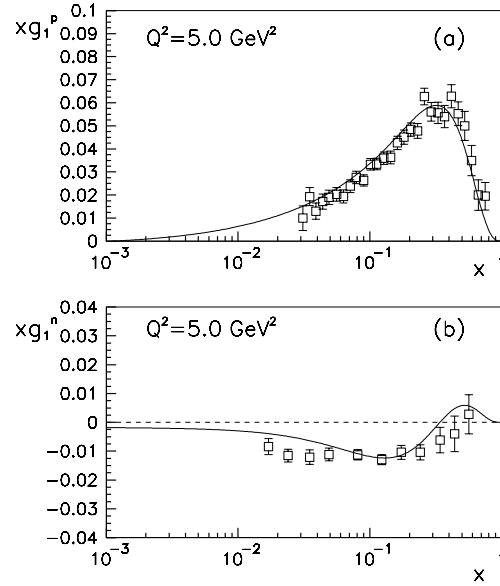


Figure 2: Fitting the data [21] for g_1 at $Q^2 = 5 GeV^2$ using the input distributions Eqs. (2.2.1)-(2.2.6).

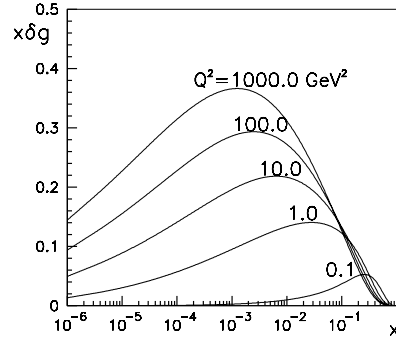


Figure 3: Predicted polarized gluon distribution $x\delta g(x, Q^2)$ in the proton at the different Q^2 -scales, which show the accumulation of radiative polarized gluons at small x in the evolution.

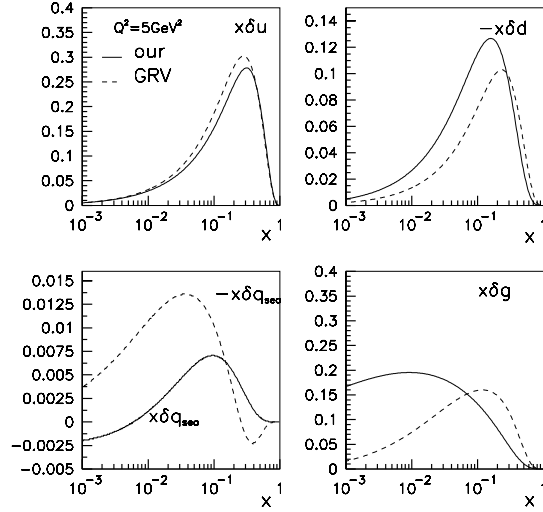


Figure 4: Comparisons of our predicted polarized LO parton distributions at $Q^2 = 5\text{GeV}^2$ with the GRV distributions [22].

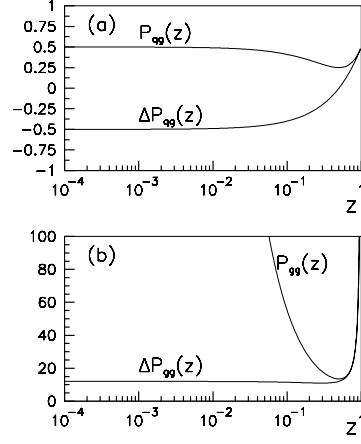


Figure 5: The splitting functions.

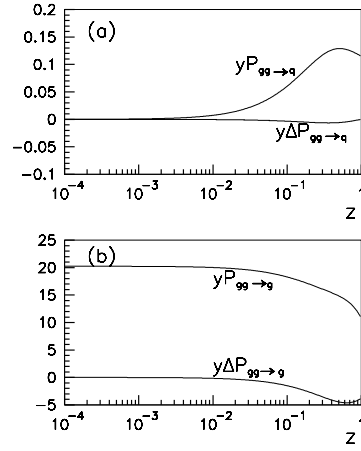


Figure 6: The recombination functions.

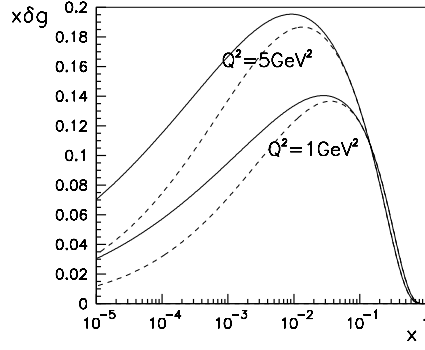


Figure 7: Predicted polarized gluon distributions $x\delta g$ in the nucleon at $Q^2 = 1$ and 5 GeV^2 with gluon recombination corrections (solid curves) and without gluon recombination corrections (dashed curves).

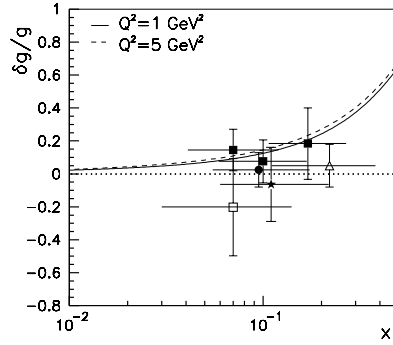


Figure 8: Comparison of dynamically predicted $\delta g/g$ with the COMPASS data [23] at $Q^2 = 1$ and 5 GeV^2 .

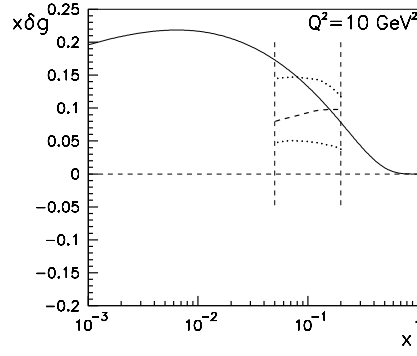


Figure 9: Our predicted $x\delta g$ at $Q^2 = 10\text{GeV}^2$ (solid curve). Broken curve is the result by DSSV using RHIC measurements in [24]; dotted curves are the fits within the 90% confidence level (C.L.) interval

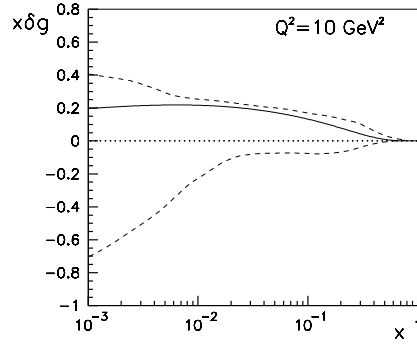


Figure 10: Comparison of dynamically predicted polarized gluon distribution with the NNPfD bounds [1].

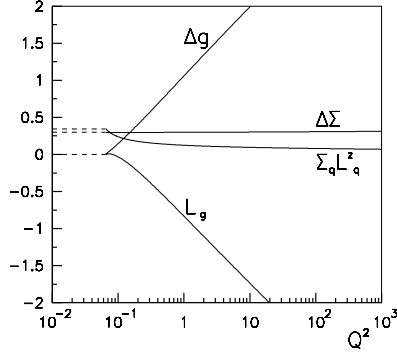


Figure 11: Contributions of spin and orbital motion of the partons to the proton spin and their evolutions with Q^2 .

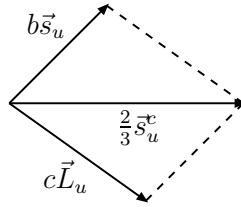


Figure 12: A schematic diagram of the proton spin crisis: Orbital angular momentum \vec{L}_u of a valence u-quark at a bound state scale μ^2 impels the direction of the u-quark spin (\vec{s}_u) to deviate the polarized direction of the proton (\vec{s}_u^c) and gives $\Delta\Sigma < 1$.

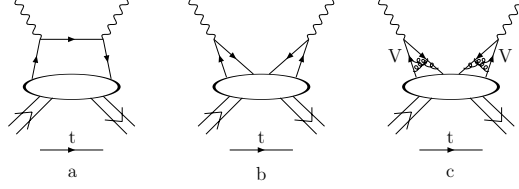


Figure 13: The time ordered decomposing of DIS diagrams. (a) The struck quarks are on-mass-shell since they have only forward component. (b) A "cat ear" diagram, which vanishes in the collinear factorization schema. (c) The "cat ear" diagram with higher order QCD corrections, which are non-vanished at low Q^2 , but can be isolated using a naive VMD model.

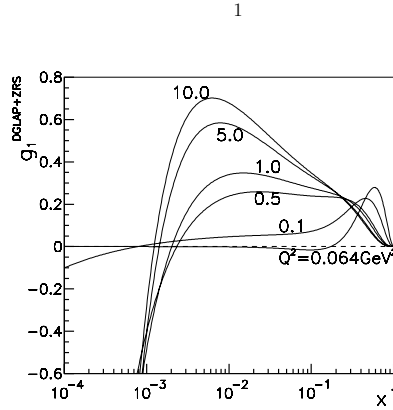


Figure 14: Perturbative $g_1^{DGLAP+ZRS}$. All partons are evolved from three valence quarks at $\mu^2 = 0.064 \text{ GeV}^2$.

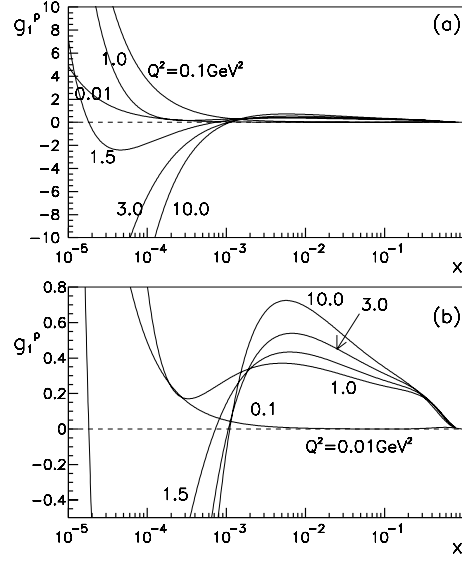


Figure 15: g_1^p evolutions at different values of Q^2 in (a) large and (b) small scales.

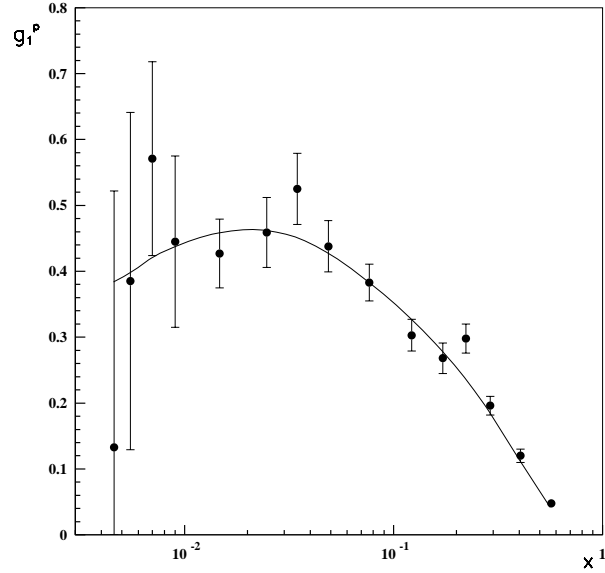


Figure 16: Predicted g_1^p at $x > 10^{-3}$ and comparisons with the COMPASS data [47]. Note that the values of $Q^2(x)$ of each measured point are different (see Table I of Ref.[29]).

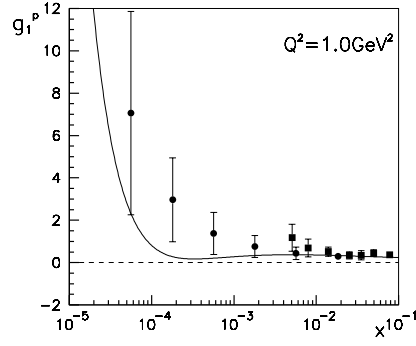


Figure 17: Predicted g_1^p at $Q^2 = 1\text{GeV}^2$ and the comparison with the HERA data [48].

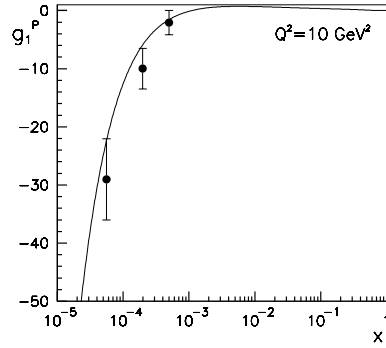


Figure 18: Predicted g_1^p at $Q^2 = 10\text{GeV}^2$ and the comparison with the HERA "data", which are based on the NLO QCD predictions with the statistical errors expected at HERA [49].

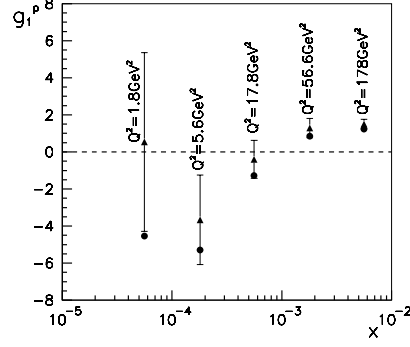


Figure 19: Predicted g_1^p at $Q^2 = 1.8\text{GeV}^2$, 5.6GeV^2 and 16.5GeV^2 at $x < 10^{-3}$ (circles) and the comparison with the HERA data (triangles).

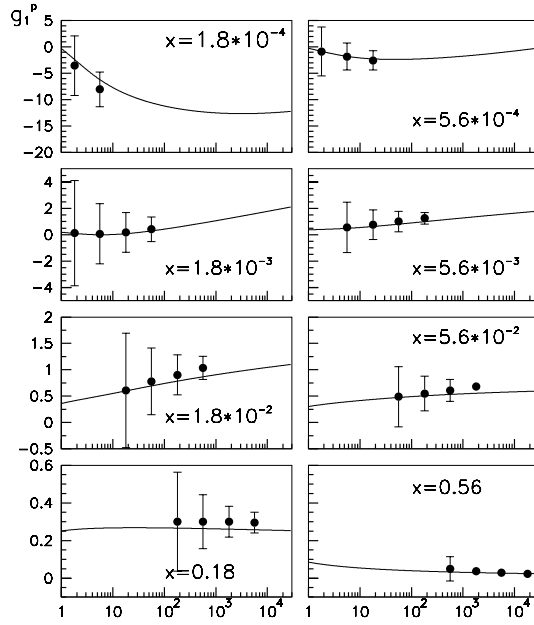


Figure 20: Predicted Q^2 -dependence of g_1^p with fixed values of x . The data are taken from [50].

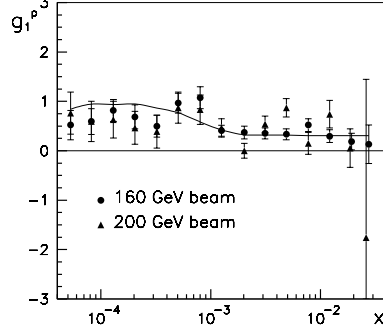


Figure 21: Predicted g_1^p as a function of x with different measured $Q^2(x)$ (solid curve). Note that the low values of x connect with the low values of $Q^2(x)$. The data are taken from COMPASS primary results with two different beam energies [14,15,16,17,18].

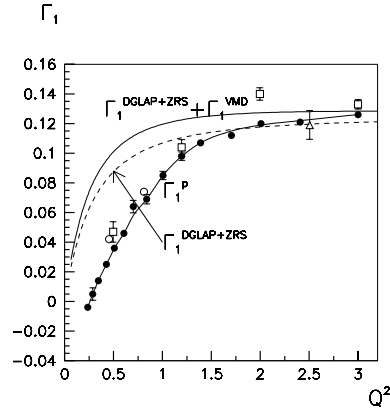


Figure 22: Contribution of quark helicity $\Gamma_1^{DGLAP+ZRS}(Q^2)$ (dashed curve) and combining VMD contribution $\Gamma_1^{DGLAP+ZRS}(Q^2) + \Gamma_1^{VMD}(Q^2)$ (solid curve). The data are taken from Hermes experiment at DESY [92,93], the E143 experiment at SLAC [94] and the EG1a experiment using the CLAS detector at JLab [95,96,97,98].

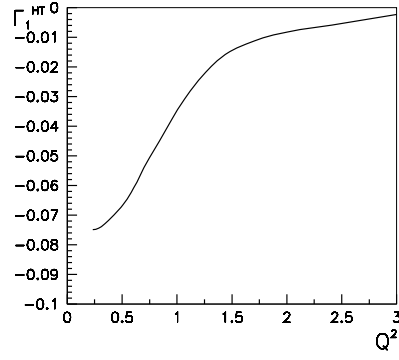


Figure 23: Contribution of higher twist $\Gamma_1^{HT}(Q^2)$ (smoothed curve) is taken from data-
 $[\Gamma_1^{DGLAP+ZRS}(Q^2) + \Gamma_1^{VMD}(Q^2)]$.

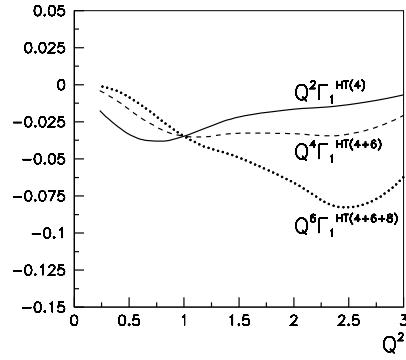


Figure 24: Three different analysis of the higher twist contributions.

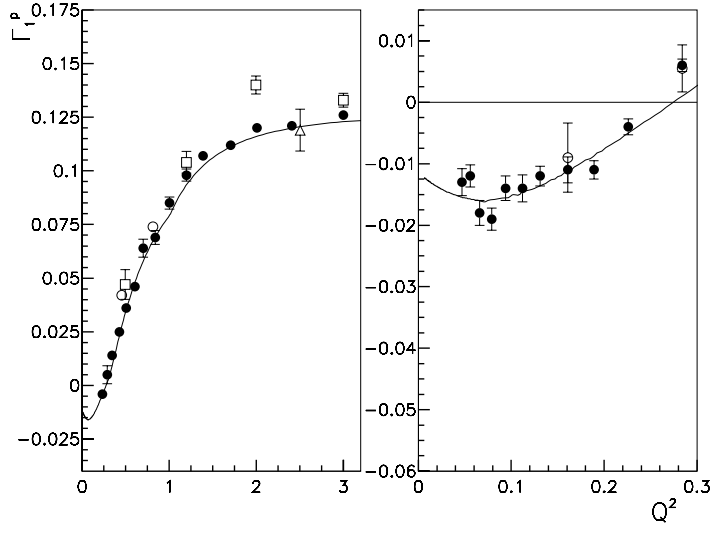


Figure 25: The Q^2 dependence of $\Gamma_1^p(Q^2)$ calculated by Eqs. (4.2.6) and (4.2.7). The data are taken from [92,93,94,95,96,97,98].

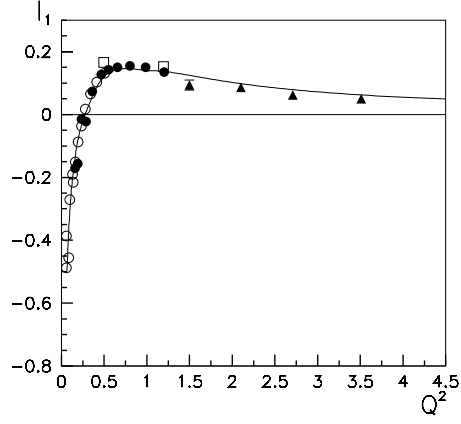


Figure 26: The Q^2 dependence of $I_1^p(Q^2)$ calculated by Eq. (4.1.3). The data are taken from [92,93,94,95,96,97,98].